Reconfigurable MIMO Antenna for IoT Wireless Applications Controlled by Embedded System

Naresh Kumar[1], Pradeep Kumar[1], and Manish Sharma[2]

[1]*JC Bose University of Science & Technology (YMCA), Faridabad, India,*
[2]*Chitkara University, Punjab, India*

https://doi.org/10.26636/jtit.2024.2.1532

Abstract — In this paper, a reconfigurable 2×2 and 4×4 MIMO antenna is designed for UWB X-band wireless applications. The proposed design uses square patch radiating electromagnetic energy and a novel ground structure and consists of a reconfigurable module enabling to set the operating mode using PIN diodes. The antenna allows rejecting 5 GHz WLAN and 7 GHz DSS interference by introducing "T–T" shape type stubs embedded on the radiating patch. The proposed design has reconfigurable features by using RF PIN diodes switch controlled by embedded module. Analysis of the proposed structure's performance shows a good agreement between simulated results and actual outcomes measured in real-worlds scenarios.

Keywords — DSS, MIMO, PIN diode, reconfigurable, UWB X band antenna, WLAN

1. Introduction

Nowadays, reconfigurable antenna circuits are gaining the attention of researchers due to the increasing demand for advanced wireless applications using multimode and multiband antenna configurations, such as wireless personal area networks (WPANs), wireless body area networks (WBANs), and short-range radar systems. Reconfigurable antennas may also be used as a multiband solution, covering different lower band applications, such as Bluetooth, UMTS, satellite uplink/downlink, WLAN, and WiMAX. The use of single element antennas causes problems with interference which needs to be mitigated by filters. On the other hand, a single element antenna system suffers from multipath feeding – a phenomenon which decreased the overall efficiency of the aerial and reduces its operating bandwidth.

Multiple-input multiple-output (MIMO) antenna systems are the prospective solution offering various features, such as large channel capacity, multipath fading immunity, and higher data transmission rates. In such types of antennas, RF PIN diodes are used as passive switches to control notched bands, thus providing the reconfigurability feature which may be also controlled remotely [1], [2]. The designed process is based on an equivalent circuit model of the antenna and a circuit theory analysis from [3].

Various techniques are used in the literature to ensure that the radiating elements, as T-shaped metal stubs in the ground [4] or fan-type decoupling structures [5] are isolated. Some design techniques are used quite commonly and, in some cases, there is no need for using any decoupling structures [6]. In [7], a dome-shaped 2×2 MIMO antenna system with T-shaped in-ground stubs and two radiating elements placed orthogonally, including two V-shaped branches, is proposed. A CPW feed dual monopole antenna with the shared Minkowski fractal effect, as well as a multiband antenna for WLAN/X-band satellite communications, with radiating elements placed orthogonally and ensuring greater isolation between radiating elements of the 2×2 MIMO antenna system, are proposed in [8]–[10].

Compact MIMO antennas for 5G applications with the size of 14×26 mm^2 and good isolation are presented in [11]. A metamaterial antenna with an electrical size of $0.29 \times 0.25\ \lambda_0$ providing dual-band operation centered at 2.48 GHz and 3.16 GHz is described in [12]. In paper [13], a Koch fractal MIMO antenna with its maple leaf fractal structure shorted with the ground is presented, while in [14] a closely placed circular radiating patch antenna embedded with T-shaped stubs and protruded strips is researched. Paper [15] demonstrates the Sierpinski carpet fractal UWB antenna with a square-shaped funeral-like ground stub with a vertical slot which provides isolation in excess of 16.3 dB.

A single band-notched MIMO antenna with a rectangular patch placed orthogonally, with an added parasitic ground structure achieving $|S_{21}| <= -20$ dB is proposed in [16]. Other antennas using the electromagnetic bandgap (EBG) structure in the same plane as the circular patch are presented in [17], while a Hilbert fractal-shaped slot which is etched in-ground, thus providing isolation of less than –18 dB is proposed in paper [18]. A WLAN notched band MIMO antenna with a rectangular patch and a rectangular in-ground stub is used to achieve higher isolation in [19]. The proposal from [20] shares common ground between two hexagonal radiating patches and the embedded T-shaped in-ground stub provides isolation better than 22 dB.

The designs showcased in articles [21]– [22] incorporate different techniques to obtain better isolation of more than 20 dB throughout the entire operating band. These techniques rely, inter alia, on orthogonal placement of the radiating patch,

Tab. 1. Optimized parameter values of the proposed antenna, obtained with the Ansys HFSS EM software simulator.

Parameter	[mm]	Parameter	[mm]	Parameter	[mm]
$L_{sub} = W_{sub}$	18.0	W_g	14.0	S_4	5.50
h_{sub}	0.79	R_1	6.00	n_1	6.50
P_1	13.0	R_2	1.80	n_2	2.52
P_2	9.00	S_L	1.25	n_3	3.75
W_m	2.00	S_W	0.5	n_4	5.00
L_m	6.00	S_1	2.40	n_5	1.75
g	1.50	S_2	7.00	t_1	0.35
L_g	2.50	S_3	5.00	t_2	0.50

using an EBG decoupling stub connected to the individual ground planes, implementing a decoupling strip and a slotted ground plane between two closely spaced radiating patches, using two F-shaped in-ground stubs, the Sierpinski fractal, two extended curved ground stubs, and a slotted funnel-shaped element added to the shared ground between two patches.

Four-port MIMO antenna configurations are reported in [23]–[33], where techniques such as the connection of a stub between the pair of the radiating patches, circular arc-shaped ground stubs, etched in-ground slots, a fan-shaped parasitic element placed centrally between four radiating patches, and double decoupling branches are utilized. The topology of the antennas is reconfigured by relying on various switching RF techniques, such as RF PIN diodes, varactor diodes, and MEMS switches. Reconfigurable antennas are essential for handheld and remotely operated devices, as they offer several important advantages, such as multiband operation, fewer filtering element dependencies, decent isolation and out-of-band signal rejection [34]–[36].

In this paper, an orthogonal arrangement of a reconfigurable radiating patch is proposed for a two/four-port MIMO antenna to achieve reconfigurability. The proposed configuration offers wide operational frequency spectrum and remote control ability thanks to embedded module. UWB-X band spectrum is efficiently utilized by the proposed MIMO antenna even in the multipath channel environment.

2. MIMO Antenna Unit Cell

This section discusses the evolution of the proposed antenna from a single port to a multi-port configuration. Figure 1 shows the layout of the proposed MIMO unit cell. The antenna is fabricated on Rogers RTDuroid substrate, with the radiating patch on one side and the ground plane on the opposite side of the substrate. Such a cell has a compact volume of 18×18×0.787 mm^3 and is connected to a matched fed microstrip line with a 50 Ω SMA connector. The configuration of the MIMO antenna unit cell, without filters, is shown in Fig. 1c.

The radiating patch is made of a rectangular patch, while the modified ground plane provides matching in wide impedance bandwidth. Two rectangular slotted ground consists of a rectangular patch along with an embedded ellipse of major radius R_1 and minor radius R_2. Figure 1d shows the final version of the single unit MIMO cell, where two lots with an area of $S_1 \times S_2$ and one slot with an area of $S_3 \times S_4$ are etched on the radiating patch. A pair of a Γ-shaped and an inverted T-shaped stubs is embedded to eliminate interference in WLAN and DSS bands. The key dimensions are shown in Fig. 1 and are summarized in Tab. 1.

Tab. 2. Reconfigurable modes of the proposed dual notched band antenna.

Mode	PIN diodes			Notched bands		Operating bandwidth [GHz]
	D1	D2	D3	WLAN [GHz]	DSS [GHz]	
1	off	off	off	-	-	3.95–12.63
2	on	off	off	5.14–5.59	-	3.82–11.27
3	off	on	on	-	7.32–7.76	3.90–12.51
4	on	on	on	5.10–5.68	7.23–7.83	3.72–11.54

The proposed UWB X band unit MIMO cell is developed into three different antennas shown in Fig. 2a. Initially, a radiating patch with the dimensions of $P_1 \times P_2$ and a rectangular ground plane with the size of $L_g \times W_g$ incorporated in antenna A is designed. It offers an impedance bandwidth of 3.24–6.07 GHz. Antenna B has an additional ellipse which increases the bandwidth to 3.74–11.72 GHz. Antenna C is the final version and is obtained by etching a pair of rectangular slots in the ground plane. Such a technique offers an impedance bandwidth of 3.96–12.69 GHz and results in more efficient impedance matching compared to the previous versions.

To remove the undesired interference from other bands, stubs are positioned on the slotted rectangular radiating patch of the antenna. The Γ-shaped stub removes interfering WLAN frequencies and the rotated T-shaped stub eliminates DSS interference. The resonance frequency f_m of each notched band is calculated by [27]:

$$f_m = \frac{c}{2L_{sn}\sqrt{\varepsilon_{reff}}}, \tag{1}$$

where c is the speed of light, L_{sn} is the total length of the stub and ε_{reff} is the effective dielectric constant of the substrate given by:

$$\varepsilon_{reff} = \frac{\varepsilon_r + 1}{2}, \tag{2}$$

where ε_r is the dielectric constant of the substrate used.

Surface current density at notched bands centered at 3.60 GHz and 7.50 GHz is presented in Fig. 3a-b. In both cases, the maximum surface current density concentration exists within the Γ–T shaped stubs, which are responsible for notching interfering WLAN and DSS bands. At these frequencies, the antenna is characterized by both high and low impedance, leading to band-stop filtering characteristics, where the entire interfering input signal is reflected instead of being radiated.

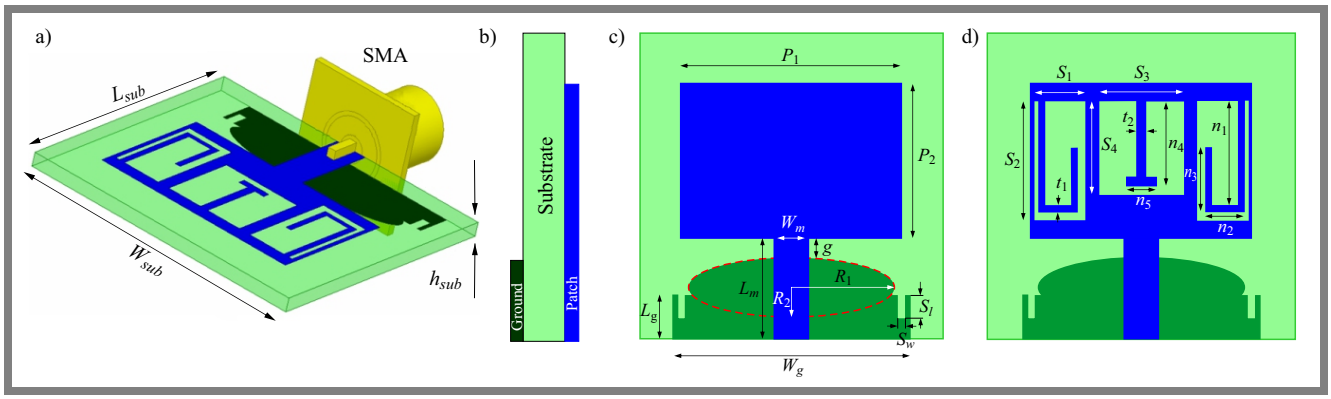

Fig. 1. MIMO unit cell designed: a) inclined view of the antenna with SMA feed, b) side view, c) unit cell with notched bands, and d) unit cell without notched bands.

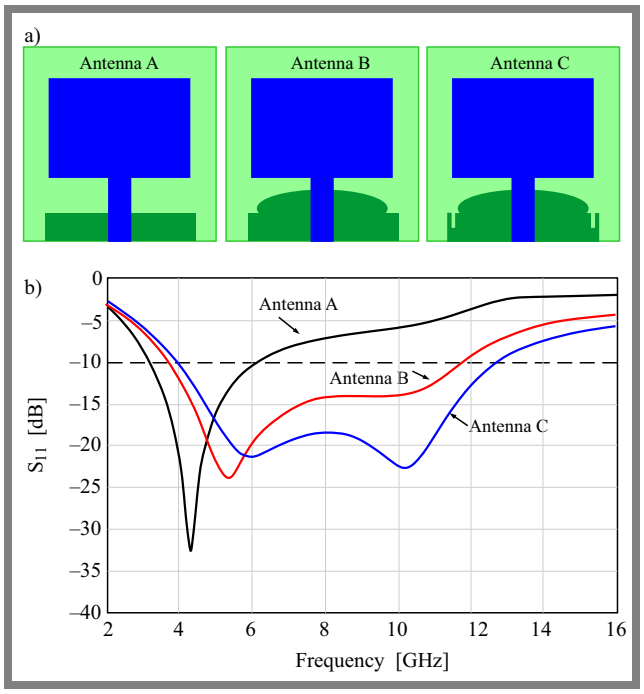

Fig. 2. Design steps of MIMO unit cell a) and S_{11} of all antennas b).

Figure 3c-d shows that by varying the physical length of the stubs, bandwidth may be shifted from lower to higher frequency and, hence, the trimming the resonance frequency is possible. For the WLAN notched band, the overall length of the Γ-shaped stub is:

$$WLAN = n_1 + n_2 + n_3 \ \text{[mm]} \ , \tag{3}$$

Similarly, for the DSS notched band, the total length of the T stub is given by:

$$DSS = n_4 + n_5 \ . \tag{4}$$

A change in n_3 length from 3.25 to 4.25 mm causes the bandwidth to shift from 3.46–3.92 GHz to 5.06–5.52 GHz, with a corresponding maximum value of VSWRs of 53.91 (at 5.69 GHz) and 30.28 (at 5.30 GHz). By varying n_5 length from 1.75 to 2.25 mm, DSS notched band bandwidth shifts from 7.25–7.76 GHz with the maximum VSWR of 10.38 at 7.60 GHz, to 6.77–7.23 GHz with the maximum VSWR level of 16.84 at 7.04 GHz. The optimized values for WLAN and DSS bands are found to be $n_3 = 3.75$ mm – resulting in a bandwidth of 5.33–5.81 GHz and the maximum VSWR of 14.29 at 5.61 GHz, and $n_5 = 1.75$ mm – resulting in a bandwidth of 7.25–7.76 GHz and the maximum VSWR of 10.38 at 7.60 GHz.

It should be noted that during the optimization of each notched band, no negative impact is exerted on the bandwidth of the other band, as the physical length of the stub remains constant, while the remaining dimensions are varied.

2.1. RF Switching Circuit

Reconfigurable antennas are capable of tuning the operating frequency, as well as changing the polarization or phase through radiation patch modifications, for instance with the use of various RF switching components, such as PIN diodes.

Thanks to its reconfiguration capabilities, the proposed antenna operates in the 3.95–12.63 GHz frequency range, i.e. in "wideband operation" mode 1. The second operating mode is in the 3.82–11.27 GHz band, while the third operating band is 3.90–12.51 GHz. Another operating mode involves rejecting the 3.72–11.54 GHz band with interfering WLAN and DSS signals (Tab. 2).

Figure 4 illustrates the input impedance of the proposed antenna (without and with notched bands). Figure 4a presents the impedance of a MIMO unit cell without the inclusion of interfering bands. The real impedance of the antenna follows a nearly constant 50 Ω curve, while the imaginary part follows a 0 Ω impedance curve in the entire operating band. Figure 4b depicts both real and imaginary impendence components for the proposed dual notched band MIMO unit cell. The maximum real component values for WLAN and DSS equal 5.13 Ω (5.63 GHz) and 5.62 Ω (7.59 GHz), respectively. For both of the notched bands, the imaginary impedance component shifts from negative to positive values. For the remaining bandwidth, real and imaginary values equal nearly 50 Ω and 0 Ω, respectively.

Figure 4c shows a prototype of the proposed antenna with the switching diodes, while Fig. 4d shows reconfigurable characteristics of the MIMO unit cell antenna.

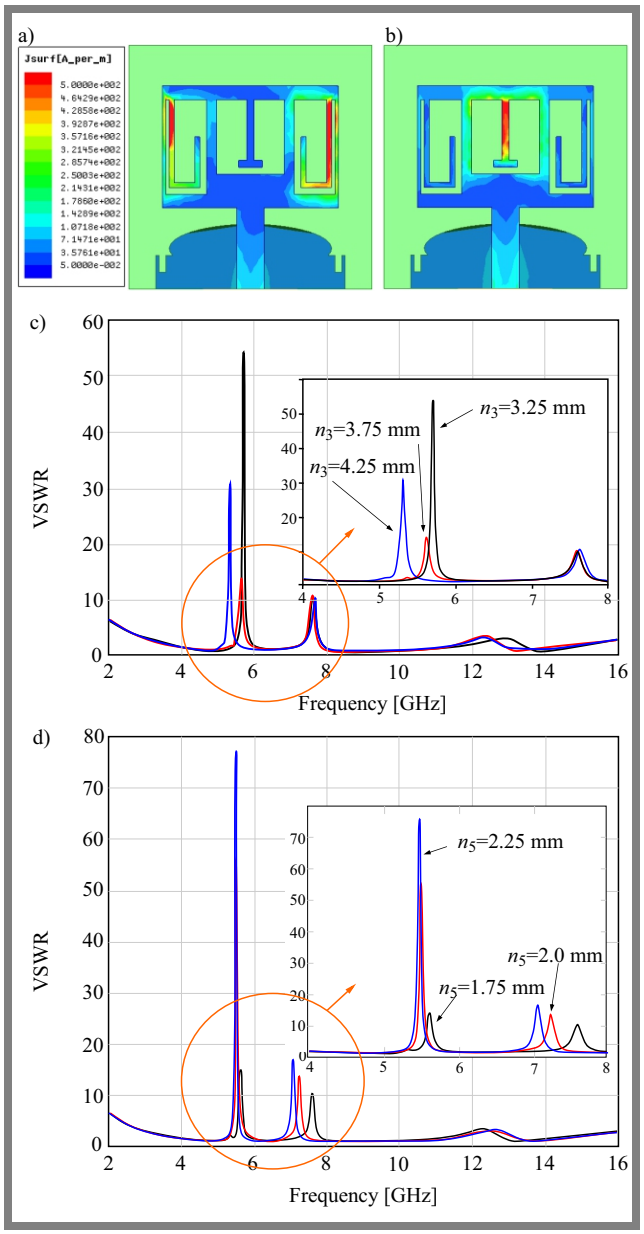

Fig. 3. Surface current density at 5.60 GHz a), surface current density at 7.50 GHz b), physical length variation of WLAN stub n_5 c), and physical length variation of DSS stub n_5 d).

3. 2×2 MIMO Antenna Design

Based on the developed unit cell, in the next step a 2×2 MIMO antenna was designed. It occupies an area of $L_{sub} \times 2W_{sub}$ mm^2 without compromising operational bandwidth and while maintaining the notched band functionality.

An important observation can be derived that without any isolation techniques applied between two ports, isolation of over 20 dB is maintained between both ports, as shown in Fig. 5c-d. Figure 5f-g shows the surface current density distribution. In comparison with Fig. 3a-b, the maximum surface current density levels are concentrated within Γ- and inverted T-shaped stubs. This distribution of current density is carried out at center notched frequencies of 5.50 GHz and 7.50 GHz, respectively.

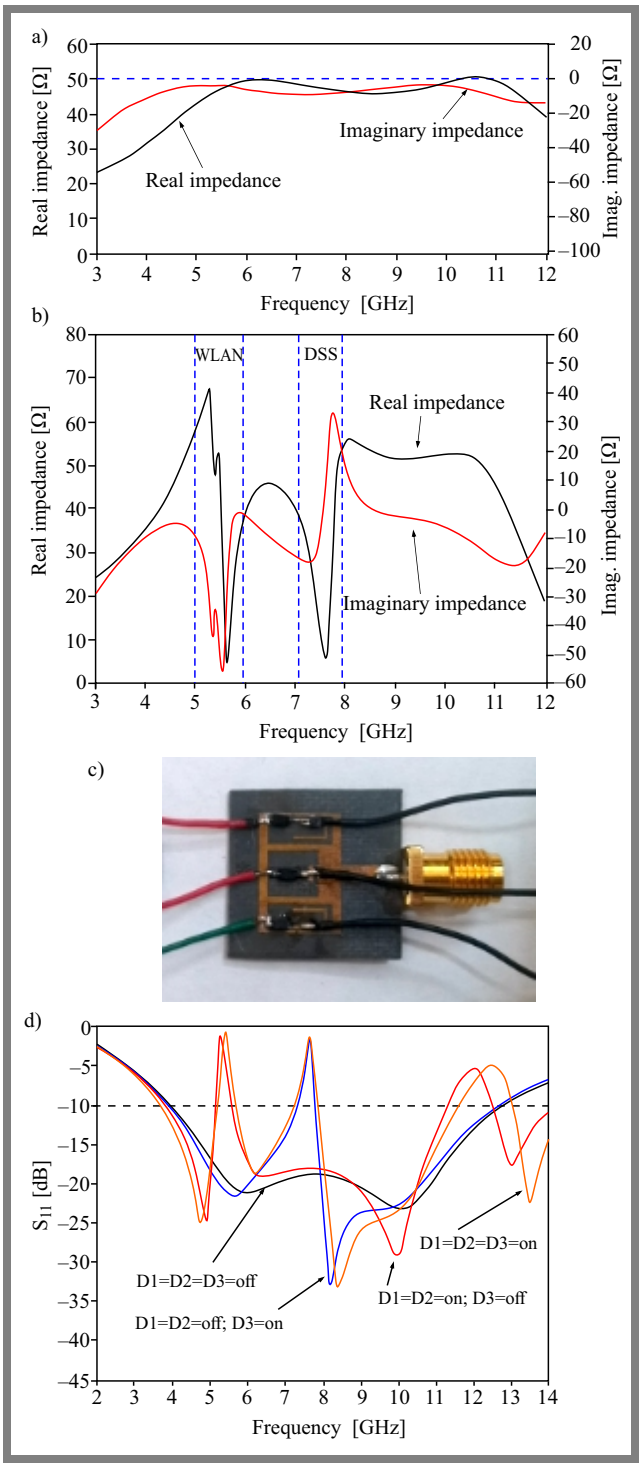

Fig. 4. Antenna impedance without filters a), impedance with filters b), prototype with PIN diodes c), s parameters for different switching modes d).

3.1. Performance of the 2×2 Configuration

To validate the proposed antenna array design, several important parameters are determined during the simulations. First, a parameter that is critical for the evaluation of the entire system, namely the envelope correlation coefficient (ECC), is calculated. This parameter is expressed, in terms of the radiation field pattern, as:

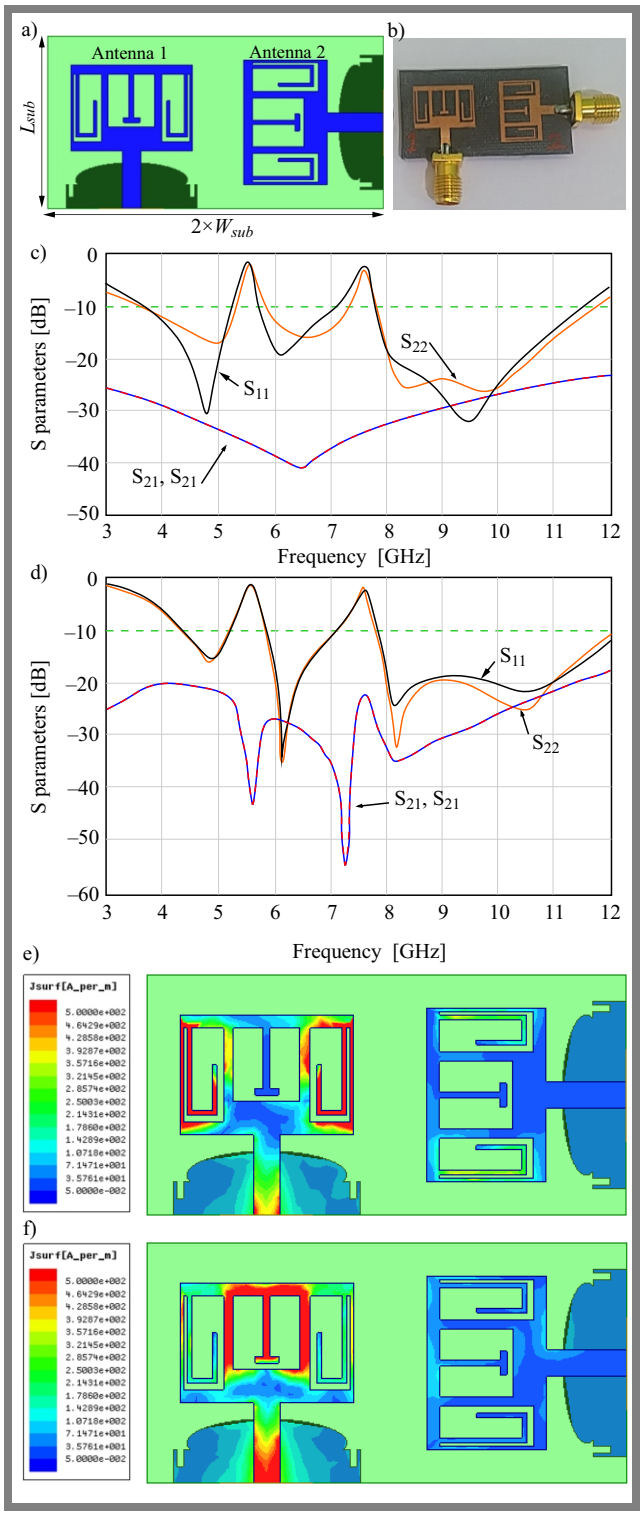

Fig. 5. 2×2 MIMO dual notched band antenna: a) designed using HFSS software, b) view of the prototype's radiating side, c) S parameters (simulated), d) S parameters (measured), e) simulated SFD at 5.50 GHz, and f) simulated SFD at 7.50 GHz.

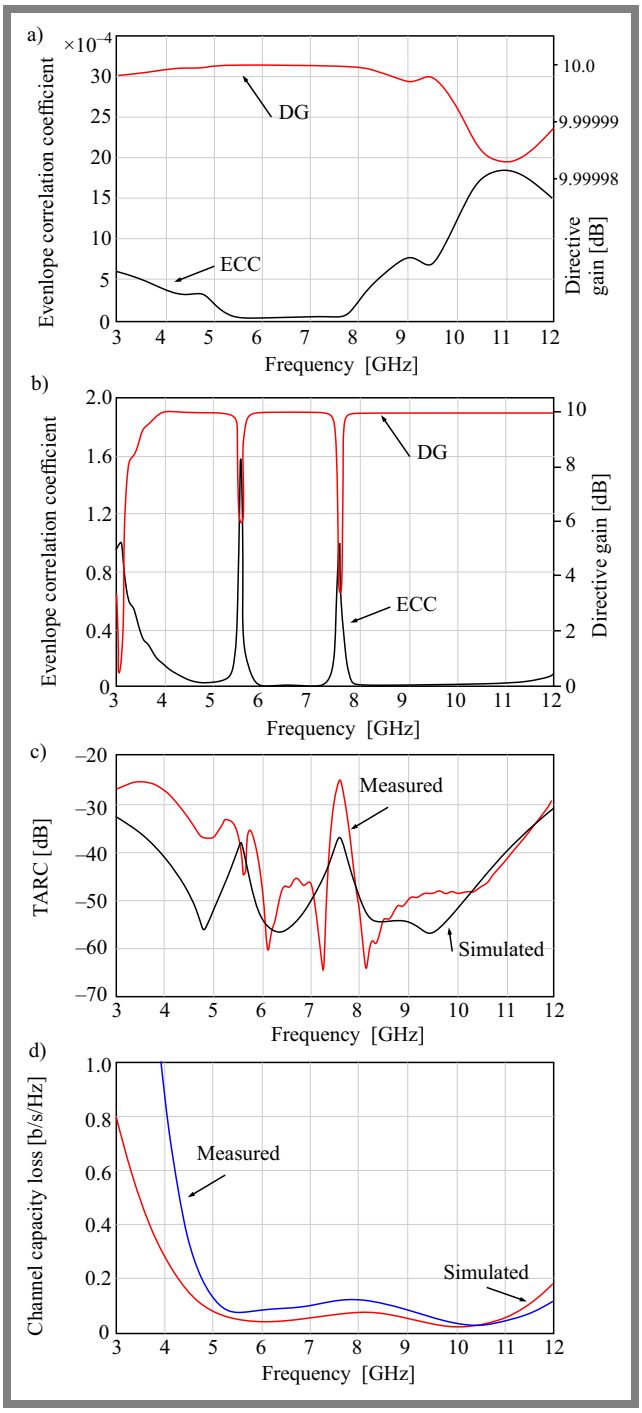

Fig. 6. Performance of the proposed 2×2 MIMO antenna: a) ECC and DG simulated, b) ECC and DG measured, c) TARC, and d) channel capacity loss.

$$\rho_e = \frac{\left| \iint_{4\pi} [\overrightarrow{F}_1(\theta,\phi) \times \overrightarrow{F}_2^*(\theta,\phi)]\, d\Omega \right|^2}{\iint_{4\Omega} \left|\overrightarrow{F}_1(\theta,\phi)\right|^2 d\Omega \left|\overrightarrow{F}_2(\theta,\phi)\right|^2 d\Omega}, \tag{5}$$

where $\overrightarrow{F}_1(\theta,\phi)$ determines the radiation field pattern with one port being excited and all other remaining ports being terminated with 50 Ω impedance. For a system with N antennas, ECC between any two antennas i and j is given by:

$$\rho_e(i,j,N) = \frac{\left|C_{i,j}(N)\right|^2}{\prod_{k=i,j}\left[1 - C_{k,k}(N)\right]}, \tag{6}$$

where $C_{i,j}(N)$ is:

$$C_{i,j}(N) = \sum_{n=1}^{N} S_{i,n}^{*} S_{n,j} \ . \tag{7}$$

From Eqs. (6) and (7):

$$\rho_e(i,j,N) = \frac{\left| \sum_{n=1}^{N} S_{i,n}^{*} S_{n,j} \right|^2}{\prod_{k=i,j} \left[1 - \sum_{n=1}^{N} S_{k,n}^{*} S_{n,k} \right]} \ . \tag{8}$$

For a 2×2 MIMO dual notched band MIMO antenna, the ECC is:

$$ECC = \frac{\left| S_{11}^{*} S_{12} + S_{21}^{*} S_{22} \right|^2}{\left(1 - |S_{11}|^2 - |S_{21}|^2\right)\left(1 - |S_{22}|^2 - |S_{12}|^2\right)} \ . \tag{9}$$

For any uncorrelated MIMO configuration, the ideal value of ECC is zero, but in a real-world system, such a value should be below 0.2. For the proposed MIMO antenna configuration, as shown in Fig. 6a-b, the ECC value (both simulated and measured) is well below 0.2. There is a peak rise at notched bandwidth, and it is caused by the non-radiating mode of the antenna.

Directive gain is another parameter which determines the performance of any MIMO system:

$$DG = 10\sqrt{1 - \rho_e^2} \ . \tag{10}$$

DG depends on ECC and its expected values should be over 9.95 dB within the entire operating bandwidth. In the proposed antenna, simulated and measured DG values are above 9.95 dB, as shown in Fig. 6a-b.

The placement of the antenna system (with either adjacent or orthogonal configuration used) may affect the performance of the MIMO cell. Reflection and transmission coefficients cannot influence the performance of the MIMO system and, hence, another metric, known as total active reflection coefficient based on s parameters, is introduced as:

$$TARC = \sqrt{\frac{(S_{11} + S_{12})^2 + (S_{21} + S_{22})^2}{2}} \ . \tag{11}$$

For the MIMO antenna configuration, $TARC < 0$ dB is expected and, in this design case, values lower than –40 dB and –20 dB are achieved, as shown in Fig. 6c.

Channel capacity is a parameter enabling a reliable signal transmission performed with the maximum ate available in the channel used. In such terms, channel capacity loss (CCL) is calculated by:

$$CL_{oss} = -\log_2\left(\psi^M\right) \ , \tag{12}$$

where:

$$\psi^R = \begin{bmatrix} \psi_{11} & \psi_{12} \\ \psi_{21} & \psi_{22} \end{bmatrix} \ , \tag{13}$$

$$\psi_{11} = 1 - \left[|S_{11}|^2 + |S_{12}|^2 \right] \ , \tag{14}$$

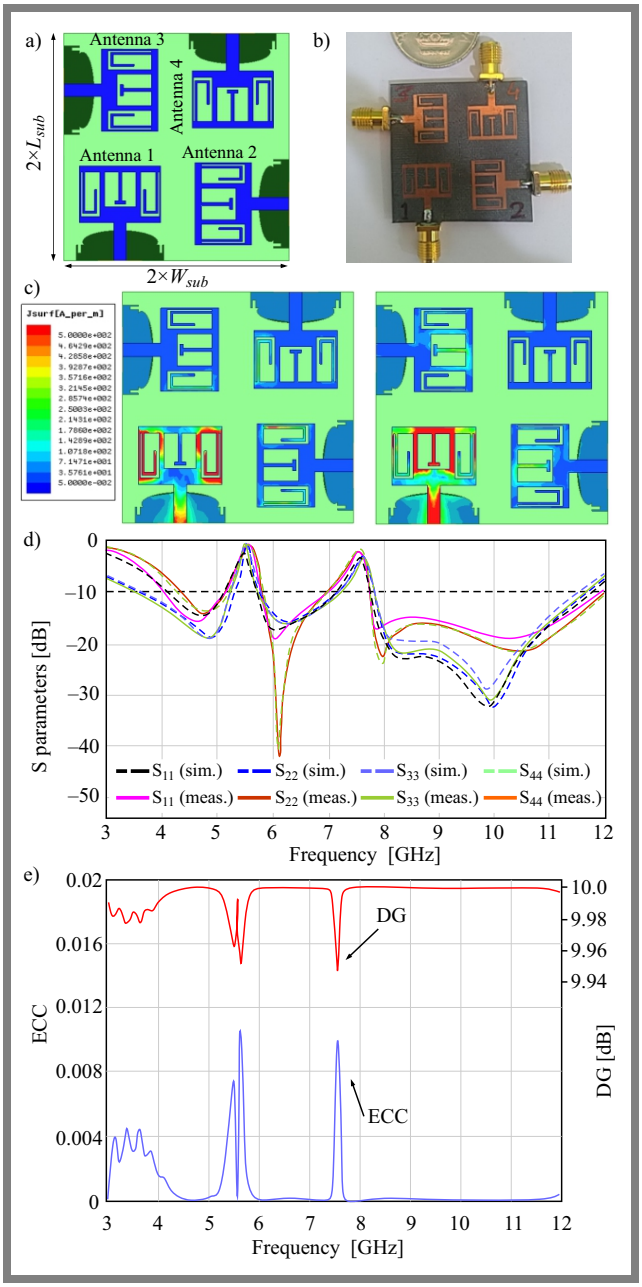

Fig. 7. 4×4 MIMO antenna configuration: a) simulated environment, b) prototype, c) SCFD at 5.56 GHz and 7.66 GHz, d) simulated and measured S parameters, and e) measured DCC and DG.

$$\psi_{22} = 1 - \left[|S_{22}|^2 + |S_{21}|^2 \right] \ , \tag{15}$$

$$\psi_{12} = -\left\lfloor S_{11}^{*} S_{12} + S_{21}^{*} S_{12} \right\rfloor \ , \tag{16}$$

$$\psi_{21} = -\left\lfloor S_{22}^{*} S_{21} + S_{12}^{*} S_{21} \right\rfloor \ . \tag{17}$$

The maximum acceptable values of CLL should below 0.4 bits/s/Hz. In the proposed solution, CLL does not exceed 0.2 bits/s/Hz, as shown in Fig. 6d.

Tab. 3. Comparison of simulated and measured VSWR values.

	WLAN [GHz]	DSS [GHz]	Bandwidth [GHz]
Simulated	5.28–5.72	7.32–7.83	3.43–11.76
Measured	5.178–5.78	7.11–7.754	4.02–12.0

4. 4×4 MIMO Antenna

Figure 7 shows the designed 4×4 MIMO antenna as an improvement of the proposed 2×2 MIMO antenna from Fig. 5. It contains four radiating patches placed orthogonally, without any isolation techniques used between the radiating elements. Figure 7c shows the surface current density for notched bands, WLAN, and DSS.

The surface current density for the proposed 4×4 MIMO antenna is simulated at 5.56 GHz and 7.66 GHz, showing that the maximum concentration of surface current is present within Γ-T stubs. The reflection coefficient shown in Fig. 7d confirms a good match between simulated and measured results. It is worth noting that port 1 – corresponding to antenna 1 – is excited in the cases, while the remaining ports (2–4) are terminated.

Figure 7e shows the measured ECC and DG values, where ECC does not exceed 0.2 and DG is over 9.95 dB.

5. Discussion of Results

Table 3 compares the VSWR results obtained during simulations and in the course of actual measurements. Slight variations may be noticed which are caused by the degree of precision obtained while fabricating the prototype. Figure 8 shows VSWR, the gain of the proposed antenna, and its radiation efficiency. The gain of the antenna maintains almost a constant value of 3.58–4.95 dBi without filters, and of 3.08–4.89 dBi with filters.

Peak gain values show a dip in the notched bands to –21.96 dB at 5.66 GHz and –14.92 dB at 7.41 GHz. The antenna's radiation efficiency varies between 70–89% within the operating band, while the efficiency of 23% and 19%, respectively, is observed in the notched bands. Far-field radiation patterns for 4.50, 6.85, and 10.20 GHz frequencies show that the monopole emitter offers a dipole pattern in the E plane, while the H plane maintains an omni-directional pattern.

Table 4 shows a comparison between the proposed MIMO antenna and other designs. Observations of the proposed design show that a considerable reduction in the size of the antenna has been achieved, all the required near- and far-field parameters and good diversity performance maintained.

6. Conclusions

In this work, reconfigurable 2×2 and 4×4 MIMO antennas for the UWB X band are proposed. Wideband operation is achieved by using a rectangular ground with two notched bands obtained by using Γ–T shaped stubs. Both measured and simulated values of the S parameter, VSWR, isolation, ECC, DG, CCL, as well as the antennas' radiating efficiency, gain and radiation patterns are investigate. Their comparison shows that all parameters lie within the acceptable range. This

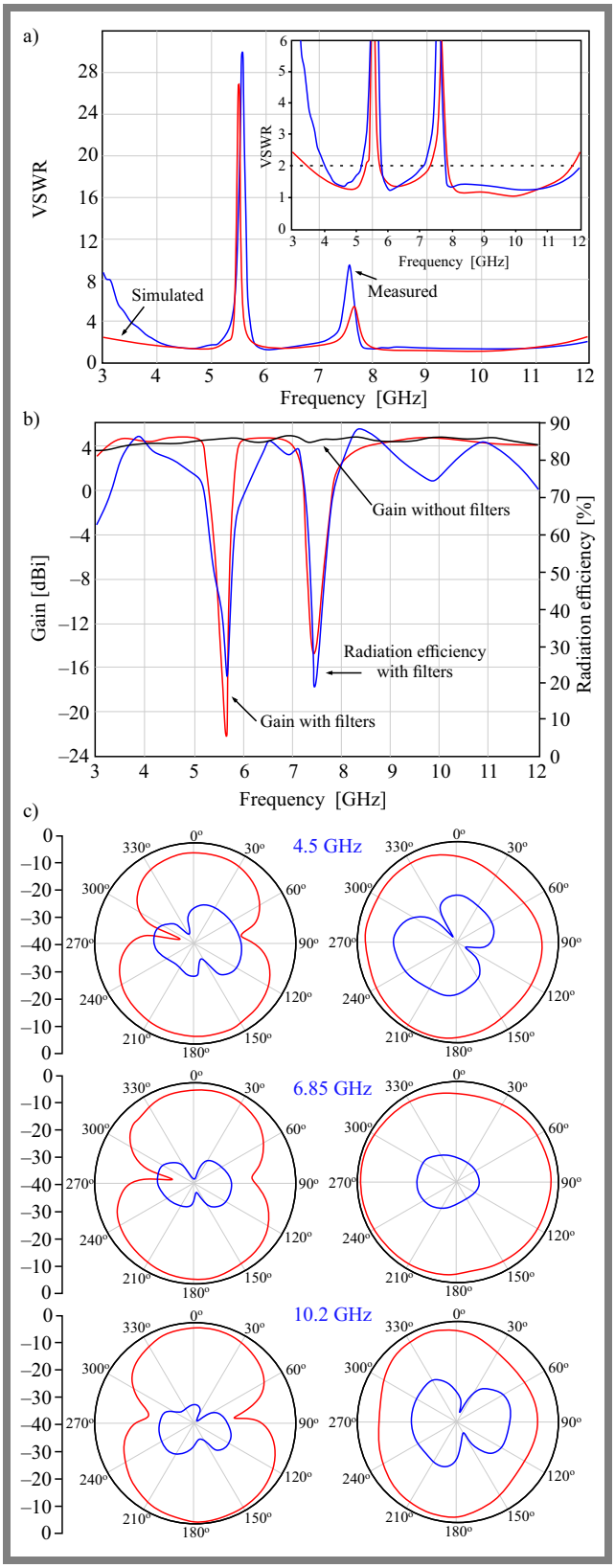

Fig. 8. VSWR a), gain b), and far-field radiation patterns at 4.50 GHz, 6.85 GHz, 10.20 GHz c).

Tab. 4. Comparison of the proposed work and other designs (P – proposed).

Ref.	No. of ports	Antenna size [mm^3]	Bandwidth [GHz]	Notched bands	ECC	DG [dB]	CCL [bits/s/Hz]	Isolation [dB]	Gain [dBi]
[23]	4	80×80×1.52	3.18–11.50	NA	<0.015	>9.95	NA	>20	5.2–9
[24]	4	48×34×1.60	3.52–10.08	NA	<0.04	NA	<0.29	>23	1.8–3
[25]	4	42×25×1.57	3.00–12.0	NA	<0.004	>9.95	NA	>15	3–5.5
[26]	4	38×38×0.80	3.00–13.20	WLAN	<0.02	NA	NA	>17	0.5–6.3
[27]	4	67×67×1.60	3.50–20.0	WLAN	<0.01	>9.95	NA	>20	4–10
[28]	4	31×31×1.60	2.00–10.60	NA	<0.005	>9.95	NA	>15	5–7
[29]	4	50×50×0.79	2.40–11.4	WiMAX WLAN	<0.05	NA	NA	>20	0.4–9
[30]	4	40×40×1.60	3.00–18.0	WiMAX	<0.03	NA	NA	>20	1.5–4
[31]	4	72×72×0.80	2.80–13.30	WiMAX WLAN	<0.06	>9.95	NA	>18	4–6
[33]	4	40×40×1.60	2.60–10.60	WiMAX WLAN	<0.01	NA	<0.40	NA	NA
P	2	18×36×0.79	3.88–12.22	WLAN X Band	<0.03	>9.95	<0.18	>20	NA
P	4	36×36×0.79	4.02–12.02	WLAN X Band	<0002	>9.95	NA	>15	3.08–4.89

analysis performed also proved that the proposed design is a potential candidate for UWB and X band systems used in remotely placed IoT applications.

References

[1] M.I. Magray *et al.*, "Compact Frequency Reconfigurable Triple Band Notched Monopole Antenna for Ultrawideband Applications", *International Journal of RF and Microwave Computer-Aided Engineering*, vol. 29, no. 11, art. no. 21942, 2019 (https://doi.org/10.1002/mmce.21942).

[2] R. Mathur and S. Dwari, "Compact Planar Reconfigurable UWB-MIMO Antenna with On-demand Worldwide Interoperability for Microwave Access/wireless Local Area Network Rejection", *IET Microwaves, Antennas & Propagation*, vol. 13, no. 10, pp. 1684–1689, 2019 (https://doi.org/10.1049/iet-map.2018.6048).

[3] M. Sharma, Y.K. Awasthi, and H. Singh, "Planar High Rejection Dual Band-notch UWB Antenna with X & Ku-bands Wireless Applications", *International Journal of Microwave and Wireless Technologies*, vol. 9, no. 8, pp. 1725–1733, 2017 (https://doi.org/10.1017/s1759078717000393).

[4] L. Wu, H. Lyu, H. Yu, and J. Xu, "Design of a Miniaturized UWB-MIMO Antenna with Four Notched-Band Characteristics", *Frequenz*, vol. 73, no. 7–8, pp. 245–252, 2019 (https://doi.org/10.1515/freq-2018-0227).

[5] L. Wang *et al.*, "Compact UWB MIMO Antenna with High Isolation Using Fence-Type Decoupling Structure", *IEEE Antennas and Wireless Propagation Letters*, vol. 18, no. 8, pp. 1641–1645, 2019 (https://doi.org/10.1109/lawp.2019.2925857).

[6] S. Rajkumar, A.A. Amala, and K.T. Selvan, "Isolation Improvement of UWB MIMO Antenna Utilizing Molecule Fractal Antenna", *Electronics Letters*, vol. 55, no. 10, pp. 576–579, 2019 (https://doi.org/10.1049/el.2019.0592).

[7] R.N. Tiwari *et al.*, "A Low Profile Dual Band MIMO Antenna for LTE/Bluetooth/Wi-Fi/WLAN Applications", *Journal of Electromagnetic Waves and Applications*, vol. 34, no. 9, pp. 1239–1253, 2020 (https://doi.org/10.1080/09205071.2020.1716859).

[8] Z. Tang *et al.*, "Design of a Compact UWB-MIMO Antenna with High Isolation and Dual Band-notched Characteristics", *Journal of Electromagnetic Waves and Applications*, vol. 34, no. 4, pp. 500–513, 2020 (https://doi.org/10.1080/09205071.2020.1724200).

[9] J. Banerjee, A. Karmakar, R. Ghatak, and D.R. Poddar, "Compact CPW-fed UWB MIMO Antenna with a Novel Modified Minkowski Fractal Defected Ground Structure (DGS) for High Isolation and Triple Band-notch Characteristic", *Journal of Electromagnetic Waves and Applications*, vol. 31, no. 15, pp. 1550–1565, 2017 (https://doi.org/10.1080/09205071.2017.1354727).

[10] A. Dkiouak, A. Zakriti, and M. El Ouahabi, "Design of a Compact Dual-band MIMO Antenna with High Isolation for WLAN and X-band Satellite by Using Orthogonal Polarization", *Journal of Electromagnetic Waves and Applications*, vol. 34, no. 9, pp. 1254–1267, 2019 (https://doi.org/10.1080/09205071.2019.1657504).

[11] M.N. Hasan, S. Bashir, and S. Chu, "Dual Band Omnidirectional Millimeter Wave Antenna for 5G Communications", *Journal of Electromagnetic Waves and Applications*, vol. 33, no. 12, pp. 1581–1590, 2019 (https://doi.org/10.1080/09205071.2019.1617790).

[12] G. Singh *et al.*, "Design of Compact Dual-band Patch Antenna Loaded with D-shaped Complementary Split Ring Resonator", *Journal of Electromagnetic Waves and Applications*, vol. 33, no. 16, pp. 2096–2111, 2019 (https://doi.org/10.1080/09205071.2019.1663274).

[13] A. Gorai and R. Ghatak, "Utilization of Shorted Fractal Resonator Topology for High Isolation and ELC Resonator for Band Suppression in Compact MIMO UWB Antenna", *AEU – International Journal of Electronics and Communications*, vol. 113, art. no. 152978, 2020 (https://doi.org/10.1016/j.aeue.2019.152978).

[14] T. Addepalli and V.R. Anitha, "A Very Compact and Closely Spaced Circular Shaped UWB MIMO Antenna with Improved Isolation, *AEU – International Journal of Electronics and Communications*, vol. 114, art. no. 153016, 2020 (https://doi.org/10.1016/j.aeue.2019.153016).

[15] R. Gurjar, D.K. Upadhyay, B.K. Kanaujia, and A. Kumar, "A Compact Modified Sierpinski Carpet Fractal UWB MIMO Antenna with Square-shaped Funnel-like Ground Stub", *AEU – International Journal of Electronics and Communications*, vol. 117, art. no. 153126, 2020 (https://doi.org/10.1016/j.aeue.2020.153126).

[16] B. Azarm *et al.*, "On Development of a MIMO Antenna for Coupling Reduction and WiMAX Suppression Purposes", *AEU – International Journal of Electronics and Communications*, vol. 99, pp. 226–235, 2019 (https://doi.org/10.1016/j.aeue.2018.11.038).

[17] T. Dabas, D. Gangwar, B.K. Kanaujia, and A.K. Gautam, "Mutual Coupling Reduction Between Elements of UWB MIMO Antenna Using Small Size Uniplanar EBG Exhibiting Multiple Stop Bands", *AEU – International Journal of Electronics and Communications*, vol. 93, pp. 32–38, 2018 (https://doi.org/10.1016/j.aeue.2018.05.033).

[18] A. Gorai, A. Dasgupta, and R. Ghatak, "A Compact Quasi-self-complementary Dual Band Notched UWB MIMO Antenna with Enhanced Isolation Using Hilbert Fractal Slot", *AEU – International Journal of Electronics and Communications*, vol. 94, pp. 36–41, 2018 (https://doi.org/10.1016/j.aeue.2018.06.035).

[19] N. Hatami *et al.*, "High Inter-element Isolation and WLAN Filtering Mechanism: A Compact MIMO Antenna Scheme", *AEU – International Journal of Electronics and Communications*, vol. 109, pp. 43–54, 2019 (https://doi.org/10.1016/j.aeue.2019.07.001).

[20] A. Kumar *et al.*, "An Ultra-compact Two-port UWB-MIMO Antenna with Dual Band-notched Characteristics", *AEU – International Journal of Electronics and Communications*, vol. 114, art. no. 152997, 2020 (https://doi.org/10.1016/j.aeue.2019.152997).

[21] D.K. Raheja, S. Kumar, and B.K. Kanaujia, "Compact Quasi-elliptical-self-complementary Four Port Super-wideband MIMO Antenna with Dual Band Elimination Characteristics", *AEU – International Journal of Electronics and Communications*, vol. 114, art. no. 153001, 2020 (https://doi.org/10.1016/j.aeue.2019.153001).

[22] P. Prabhu and S. Malarvizhi, "Novel Double-side EBG Based Mutual Coupling Reduction for Compact Quad Port UWB MIMO Antenna", *AEU – International Journal of Electronics and Communications*, vol. 109, pp. 146–156, 2019 (https://doi.org/10.1016/j.aeue.2019.06.010).

[23] M.N. Hasan, S. Chu, and S. Bashir, "A DGS Monopole Antenna Loaded with U-shape Stub for UWB MIMO Applications", *Microwave and Optical Technology Letters*, vol. 61, no. 9, pp. 2141–2149, 2019 (https://doi.org/10.1002/mop.31877).

[24] R.N. Tiwari, P. Singh, B.K. Kanaujia, and K. Srivastava, "Neutralization Technique Based Two and Four Port High Isolation MIMO Antennas for UWB Communication", *AEU – International Journal of Electronics and Communications*, vol. 110, art. no. 152828, 2019 (https://doi.org/10.1016/j.aeue.2019.152828).

[25] R. Mathur and S. Dwari, "Compact CPW-Fed Ultrawideband MIMO Antenna Using Hexagonal Ring Monopole Antenna Elements", *AEU – International Journal of Electronics and Communications*, vol. 93, pp. 1–6, 2018 (https://doi.org/10.1016/j.aeue.2018.05.032).

[26] R. Gomez-Villanueva and H. Jardon-Aguilar, "Compact UWB Uniplanar Four-Port MIMO Antenna Array with Rejecting Band", *IEEE Antennas and Wireless Propagation Letters*, vol. 18, pp. 2543–2547, 2019 (https://doi.org/10.1109/lawp.2019.2942827).

[27] M.M. Hassan *et al.*, "A Novel UWB MIMO Antenna Array with Band Notch Characteristics Using Parasitic Decoupler", *Journal of Electromagnetic Waves and Applications*, vol. 34, no. 9, pp. 1225–1238, 2020 (https://doi.org/10.1080/09205071.2019.1682063).

[28] B. Yang, M. Chen, L. Li, "Design of a Four-element WLAN/LTE/UWB MIMO Antenna Using Half-slot Structure", *AEU – International Journal of Electronics and Communications*, vol. 93, pp. 354–359, 2018 (https://doi.org/10.1016/j.aeue.2018.05.034).

[29] H. Liu, G. Kang, and S. Jiang, "Compact Dual Band-notched UWB Multiple-input Multiple-output Antenna for Portable Applications", *Microwave and Optical Technology Letters*, vol. 62, no. 3, pp. 1215–1221, 2020 (https://doi.org/10.1002/mop.31960).

[30] Z. Tang *et al.*, "Simple Ultra-wider-bandwidth MIMO Antenna Integrated by Double Decoupling Branches and Square-ring Ground Structure", *Microwave and Optical Technology Letters*, vol. 62, no. 3, pp. 1259–1266, 2019 (https://doi.org/10.1002/mop.32122).

[31] S. Kumar *et al.*, "Multiple-input-multiple-output/diversity Antenna with Dual Band-notched Characteristics for Ultra-wideband Applications", *Microwave and Optical Technology Letters*, vol. 62, no. 1, pp. 336–345, 2019 (https://doi.org/10.1002/mop.32012).

[32] D.K. Raheja, B.K. Kanaujia, and S. Kumar, "Low Profile Four-port Super-wideband Multiple-input-multiple-output Antenna with Triple Band Rejection Characteristics", *International Journal of RF and Microwave Computer-Aided Engineering*, vol. 29, no. 10, art. no. 21831, 2019 (https://doi.org/10.1002/mmce.21831).

[33] G. Kan, W. Lin, C. Liu, and D. Zou, "An Array Antenna Based on Coplanar Parasitic Patch Structure", *Microwave and Optical Technology Letters*, vol. 60, no. 4, pp. 1016–1023, 2018 (https://doi.org/10.1002/mop.31104).

[34] N.O. Parchin *et al.*, "Recent Developments of Reconfigurable Antennas for Current and Future Wireless Communication Systems", *Electronics*, vol. 8, no. 2, 2019 (https://doi.org/10.3390/electronics8020128).

[35] N.O. Parchin *et al.*, "Reconfigurable Antennas: Switching Techniques – A Survey", *Electronics*, vol. 9, no. 2, art. no. 336, 2020 (https://doi.org/10.3390/electronics9020336).

[36] S. Genovesi *et al.*, "Frequency-Reconfigurable Microstrip Antenna with Biasing Network Driven by a PIC Microcontroller", *IEEE Antennas and Wireless Propagation Letters*, vol. 11, pp. 156–159, 2012 (https://doi.org/10.1109/lawp.2012.2185673).

Naresh Kumar, Ph.D. Scholar
Department of Electronics Engineering
https://orcid.org/0000-0003-3637-4349
E-mail: engg.tanwar86@gmail.com
JC Bose University of Science & Technology (YMCA), Faridabad, India
https://www.jcboseust.ac.in

Pradeep Kumar, Ph.D.
Department of Electronics Engineering
https://orcid.org/0000-0003-1496-5121
E-mail: pkdimri@gmail.com
JC Bose University of Science & Technology (YMCA), Faridabad, India
https://www.jcboseust.ac.in

Manish Sharma, Ph.D.
Chitkara University Institute of Engineering and Technology
https://orcid.org/0000-0002-1539-2938
E-mail: manishengineer1978@gmail.com
Chitkara University, Punjab, India
https://www.chitkara.edu.in